講座

現状と課題*

武智詩子[1)]　魚住武則[1)]　辻　貞俊[1)]

Key Words：経頭蓋磁気刺激法（transcranial magnetic stimulation；TMS）

はじめに

経頭蓋磁気刺激法（transcranial magnetic stimulation；TMS）は，痛みなく脳を刺激し，四肢の筋肉から運動誘発電位（motor evoked potential；MEP）を記録できるため，中枢神経の運動系の非侵襲的検査として広く臨床応用されている．現在ではルーチン検査としてMEP検査が行われるだけではく，運動野の興奮性や抑制性を推測するための方法も試みられ，さまざまな脳機能評価に応用されている．また連続磁気刺激法が開発され，精神神経疾患への治療に用いられるようになった．本稿では磁気刺激臨床応用における現状および安全性を中心に述べる．

TMS開発の歴史

1980年，Mertonら[1)]により，経皮的に頭部や頸部を電気刺激し，骨格筋からMEPを記録する方法が開発された．これは皮質脊髄路を評価する方法として確立したが，電気刺激による強い痛みのため普及しなかった．1985年にBarkerら[2)]が，頭部にて磁気刺激を与え，手の筋から誘発電位を記録することに成功したことにより，ほとんど苦痛なくMEPを誘発できるようになり，中枢神経の運動系の検査として飛躍的に普及した．また1990年代に刺激装置の改良が進み，TMSを連続して用いる反復経頭蓋磁気刺激法（repetitive TMS；rTMS）の方法論が確立し，rTMSにより神経活動の抑制，促通が確認されるようになり[3)]，rTMSの刺激中だけでなく刺激後にも及ぶ効果を利用して，神経・精神疾患の治療に応用することが考えられるようになった．本邦では2002年からは中枢神経磁気刺激による誘発筋電図が保険収載され，さらに臨床応用が拡大している．

TMSの原理

TMSはコイルに大きなパルス電流を流すことにより生じた，周囲の変動磁場が二次的に頭蓋内渦電流を誘導し，深部の神経組織を刺激するものである．TMSは痛みや不快感が少なく，骨などの高抵抗組織で減衰せずに深部まで刺激可能であるなどの利点がある一方で，刺激の局在性が乏しいという欠点もある．現在用いられているコイルの形状には円形コイル，8の字コイル，ダブルコーンコイルの3種類がある．円形コイルはコイル直下で誘発電流密度が最大となるため刺激部位が最も広範囲となる．8の字コイルはコイルの交点直下が最大誘導電流密度となるため刺激部位の局在

* Transcranial magnetic stimulation：current trends and issues.

[1)] 産業医科大学神経内科学教室：〒807-8555 北九州市八幡西区医生ヶ丘1-1
Utako Takechi, MD, Takenori Uozumi, MD, Sadatoshi Tsuji, MD：Department of Neurology, University of Occupational and Environmental Health

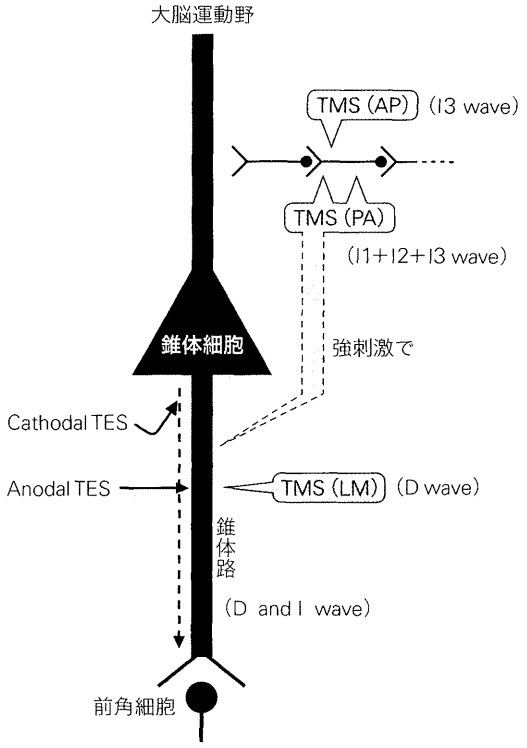

図 1　磁気刺激の機序

性はよいが，同じ位置に固定することが難しい．ダブルコーンコイルはより深部の局在的に刺激するのに適しているが，頭部の形状によってはコイルを密着できないことがある．

運動皮質を電気刺激(transcranial electric stimulation；TES) すると，錐体細胞の直接刺激による反応である direct wave (D wave) と，シナプスを介した錐体細胞の間接刺激による反応である indirect wave (I wave) とが，一連の電位として皮質脊髄路を下行する．この多重下行性インパルスが脊髄前角細胞に興奮性シナプス後電位の時間的・空間的加重を生じさせ，脊髄前角細胞の細胞膜電位を上昇させる．これが閾値を超えると，脊髄前角細胞が発火し，筋活動電位が記録される．磁気刺激の場合，弱い刺激強度では閾値の低い I wave が誘発され，強い刺激強度では D wave も生じる[4]．コイルに流れる電流の波形（単相波；monophasic か二相波；biphasic）と誘発される渦電流の方向〔後方から前方 (PA)，前方から後方 (AP)，外側から内側 (LM)〕によって大脳皮質運動野での刺激部位，あるいは D wave と I wave の賦活様式が異なる．PA 刺激では主に I waves (I1＋I2＋I3) を誘発し，強い刺激強度では低振幅の D wave も認められる．AP 刺激では I3 wave が誘発されやすく，潜時も PA 刺激より遅くなる．LM 刺激では主に D wave〔陽極性 (anodal) TES と同じ潜時〕が誘発され，PA 刺激よりも潜時が短くなる．biphasic の場合は monophasic における PA 刺激と AP 刺激を合算したものに類似するが，刺激効果は PA 刺激よりも弱い．また強い刺激強度では biphasic あるいは円形コイルを用いた刺激でも D wave が誘発されるが，その潜時は陰極性 (cathodal) TES と類似し，錐体細胞により近い刺激部位が推測されている[5]（**図 1**）．

単発 TMS による検査

一般に行われている錐体路の検査の方法は，単発の TMS によって一側の運動皮質刺激を行い，対側の骨格筋から誘発筋電図を導出するものである．主に MEP 閾値，MEP 潜時，MEP 振幅，cortical silent period (CSP) の 4 つのパラメータを測定する（**図 2, 3**）．

1．MEP 閾値

安静時 MEP 閾値は運動野の興奮性を推測するための最も簡便な手段であり，刺激強度を決めるための基準としても必要である．最初に刺激強度が最も小さく，MEP 潜時が最も短くなる刺激点を探す．その刺激点において 50～100 μV の MEP が 50%以上の確率で生じる刺激強度を求める[6]．これを安静時 MEP 閾値と呼ぶ．MEP 閾値は，安静時でも自然変動があり，高齢者や眠気がある状態では閾値は高くなり，若年者や緊張・精神活動状態では閾値が低くなる．肢位，磁気刺激装置，コイルの形状でも閾値は異なり，磁気刺激装置の最大出力の何%と表す．

2．MEP 潜時

MEP 潜時や振幅を測定する際の刺激強度は安静時 MEP 閾値の 1.1～1.5 倍の強度で行う．MEP は安静時に比較して随意収縮時に潜時が 1.5～3.0 ms 短縮し，振幅が数倍～数十倍増大する．MEP 潜時は運動皮質から標的筋に複合筋活動電位が生じるまでの時間であり，大脳運動野から脊

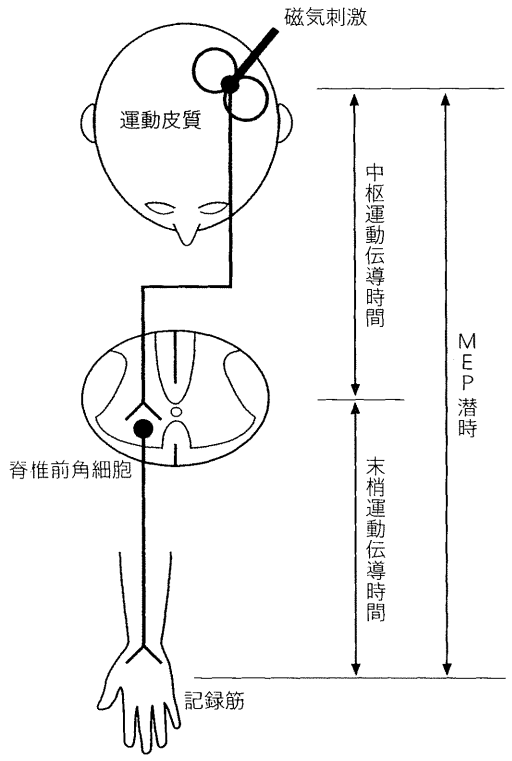

図 2　MEP 潜時

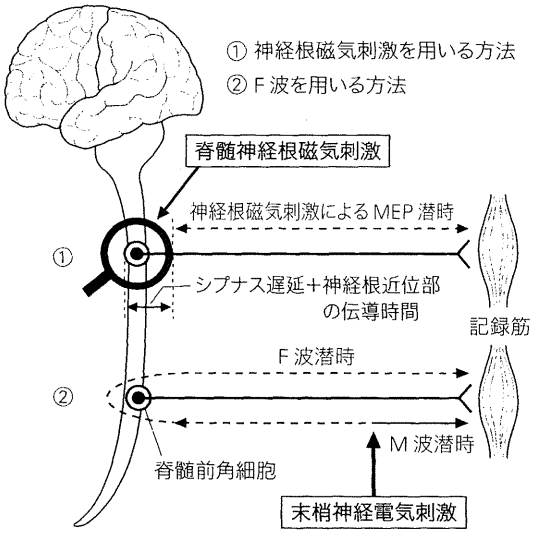

図 3　末梢運動伝導時間の計測方法

髄前角細胞までの中枢運動伝導時間（central motor conduction time；CMCT），脊髄前角細胞でのシナプス遅延（synaptic delay），脊髄から筋までの末梢運動伝導時間の 3 つに区分される（**図 2**）．末梢運動伝導時間を計測する方法としては，脊髄神経根を直接磁気刺激する方法と，標的筋の F 波潜時から計算する方法がある（**図 3**）．前者の方法で計測した CMCT には脊髄前角細胞での synaptic delay が含まれるので後者の方法が勧められる．後者は，MEP 潜時－（M 波潜時＋F 波潜時＋1）÷2 ms と計算される（1 ms は脊髄前角細胞が再興奮するのに要する時間）．CMCT は錐体路伝導時間を反映し，錐体路機能の客観的指標として最も臨床応用されている．CMCT の計測は四肢筋だけでなく顔面筋，肛門括約筋などでも可能である．また Ugawa ら[7]は脳幹部の皮質脊髄路を刺激する方法を開発し，大脳-脳幹間および脳幹-頸部間の CMCT を測定し，皮質脊髄路の病変部位の局在性をより明確に評価する方法として利用されている．

CMCT に影響する因子としては，測定時の随意収縮の有無や程度，刺激コイルの位置や方向，身長などがある．脱髄を呈する病態では CMCT の延長を来す頻度が高く，特に多発性硬化症では CMCT 延長が約 80％の患者で認められ，潜在性病変の検出にも有用性が高い．

3．MEP 振幅

MEP 振幅は個人差が大きく，MEP 潜時や CMCT より臨床的有用性は低いが，MEP 振幅と M 波振幅との比（MEP/M 波振幅比）を求めることにより，異常検出率が高くなる[6]．末梢神経や筋病変以外での MEP 振幅の低下を来す病態としては，上位運動ニューロンの脱落，錐体路の伝導ブロック，時間的分散（temporal dispersion），脊髄運動ニューロンの興奮性の低下などが考えられる．

4．cortical silent period（CSP）

随意収縮時に安静時運動閾値（resting motor threshold；RMT）以上の強度の磁気刺激を運動皮質に与えると，誘発された MEP の直後から筋活動電位の制止が観察される．これを CSP と言い，その刺激時間は主に刺激強度に依存する．持続時間のうち最初の数 10 ms は脊髄内抑制機構も関与するが，それ以降は運動皮質内抑制機構が関与す

表 1　運動野興奮性をみるための MEP 測定法と薬理学的意義

単発 TMS
運動閾値（Motor threshold；MT）：ナトリウムチャネル（Na^+channel）阻害剤で低下
MEP 振幅（MEP amplitude；MEP）：$GABA^AR$ アゴニストで低下，選択的セロトニン再取り込み阻害薬（SSRI）で上昇など
Cortical silent period；CSP）：$GABA^AR$ を反映．強刺激で $GABA^BR$ も
2 連発 TMS
短潜時皮質内抑制（Short-interval intracortical inhibition；SICI）：$GABA^AR$ を反映
皮質内促進（Intracortical facilitation；ICF）：GABA? グルタミン酸？
短潜時皮質内促進（Short-interval intracortical facilitation；SICF）：興奮性介在ニューロン（I wave 産生）
長皮質内抑制（Long-interval intracortical inhibition；LICI）：$GABA^BR$ を反映
末梢神経刺激との組み合わせ
短潜時求心性抑制（Short latency afferent inhibition；SAI）：コリン作動性？

ると考えられていて，この持続時間は運動野抑制系機能の指標の一つとして用いられている[8]．

2 連発磁気刺激法

運動皮質内の抑制機能の評価には，2 連発磁気刺激法が広く用いられている．これは一側の運動皮質に RMT 以下の条件刺激を与えた後にいろいろな刺激間隔で試験刺激を加える方法である．刺激間隔が 1～5 ms では抑制効果が認められる．10 ms 以上では促通効果が認められる[9]．また一次運動野（M1）の出力に影響を与える小脳あるいは大脳皮質領域〔対側の運動野，運動前野（PMd，PMv），補足運動野，頭頂葉後部（PPC），感覚野〕との機能結合を評価することも行われている．これらのネットワーク機能をみる方法として，その領域に TMS あるいは rTMS を条件刺激として与え，MEP への影響をみることが行われている[10]．例えば同側の運動前野に対して閾値下の単発 TMS あるいは 1 Hz rTMS を与えると MEP は振幅低下し，5 Hz rTMS では振幅増大する．これらの方法を用いてジストニアでの PMd-M1 抑制性結合低下が証明されている[11]．また，小脳に TMS を与えることにより大脳皮質運動野への TMS あるいは電気刺激により導出される MEP が抑制され，小脳失調患者では異常となることが報告されている[12]．小脳条件刺激は，ダブルコーンコイルの中心を後頭孔隆起上と外耳孔を結ぶ線上の後頭孔隆起より 3 cm 外側の部位に置く．刺激間隔 5 ms で抑制が始まり，3～4 ms 抑制が持続する．この効果は小脳刺激によって小脳皮質のプルキンエ細胞が刺激され，歯状核にインパルスが伝わり，小脳-視床-大脳皮質回路が賦活化され，皮質運動野を抑制することが推測されている．

rTMS

rTMS とは 3 発以上規則正しく反復される TMS と定義されている．rTMS には 2 種類あり，刺激頻度が 1 Hz を超えるものを高頻度 rTMS（fast rTMS），1 Hz 以下のものを低頻度 rTMS（slow rTMS）と区別している．5 Hz 以上の Fast rTMS ではコイル直下の大脳皮質の興奮性が増大し，slow rTMS では大脳皮質の興奮性は低下すると考えられている．このため，主に大脳皮質興奮性が低下している病態では fast rTMS が，逆に亢進している病態では slow rTMS が治療として用いられている．パーキンソン病患者の手の運動野に fast rTMS を行うと反応時間が改善することが報告されて[13]以降，パーキンソン病，脊髄小脳変性症，てんかんなどの神経疾患，うつ病，慢性疼痛，耳鳴り，神経因性膀胱など，さまざまな疾患に対し，rTMS が試みられている．

薬理学的にみた TMS

TMS を用いた運動野の興奮性をみる検査法は**表 1** に示すように多数開発されている．しかもその薬理学的意義もかなり解明されており，これらの方法を用いてそれらの薬理学的異常がヒトでも検討できるようになってきた[14]．これらを用いて運動障害，大脳皮質機能障害などの病態解明が行われている．

TMS の安全性

TMS の安全性については，単発あるいは 2 連発刺激に関しては重篤な副作用の報告はないが，週に 5,000 回を上限とされている．それ以上行うと聴力障害，火傷，集中力低下などが生じる可能性がある．一方，rTMS ではてんかん患者だけでな

く，正常者においてもてんかん発作を誘発する可能性が言われており[15,16]，てんかん患者には原則として禁忌である．また，rTMS では大脳皮質に強いパルス磁場を与えるため，脳動脈瘤クリッピング術後や心臓ペースメーカー埋込術後なども禁忌となる．最新の国際的な安全基準に従って，その範囲内で用いることが望まれる[17]．「日本臨床神経生理学会 磁気刺激法に関する委員会」，「磁気刺激法の臨床応用と安全性に関する研究会」が共同で3回にわたり，TMS の安全性に関する全国調査を行い，重篤な副作用がないこと，また現在までの多くの文献でも重篤な副作用はないことが報告されてはいる[18]が，実施に際しては以下の点に留意する必要がある．① 刺激のパラメータはガイドラインに従う．② 刺激中は脳波・表面筋電図のモニターを行う．③ 必ず医師が立ち会い，けいれんが生じても救急処置ができる体制をつくる．また，けいれんの閾値を下げるような薬物内服も確認する必要がある．④ 小児，妊婦などは禁忌である．頸椎症患者にも注意が必要である．⑤ 各施設における倫理審査委員会での検討，インフォームド・コンセントの取得，被験者に対する説明書なども必要である．

おわりに

磁気刺激法について検査法と連続磁気刺激の臨床応用について概説した．TMS は痛みなく大脳皮質を刺激できる唯一の方法であり，運動系の検査のみならず rTMS により神経・精神疾患に対する治療として期待が大きい．しかし対照と比較した研究が不十分であること，また報告により刺激頻度，刺激強度，刺激回数，刺激間隔などの刺激条件や刺激部位がさまざまであること，大脳皮質興奮性の変化の持続が短いことから，現在までのところ rTMS が治療法として確立されるには至っていない．rTMS の最適刺激条件と有効刺激部位が明らかになり，長期的な影響や作用機序の解明など治療法として確立すれば，神経・精神疾患に対する薬物治療の補助的治療法になりえることが期待できる．また近年 PET（positron emission tomography），MRI（magnetic resonance imaging），NIRS（near infra-red spectoroscopy）などの脳機能検査と組み合わせた研究が行われており，脳機能評価，神経ネットワークなどの研究の発展が期待される．

文 献

1) Merton PA, et al：Stimulation of the cerebral cortex in the intact human subject. *Nature* **285**：227, 1980
2) Barker AT, et al：Clinical evaluation of conduction time measurement in central motor pathways using magnetic stimulation of human brain. *Lancet* **1**：1325-1326, 1986
3) Chen R, et al：Deoression of motor cortex excitability by low-frequency transcranial magnetic stimulation. *Neurology* **48**：1398-1403, 1997
4) Day BL, et al：Electric and magnetic stimulation of human motor cortex；surface EMG and single motor unit responses. *J Physiol* **412**：449-473, 1989
5) Lazzaro VD, Ziemann U, Lemon RN：State of the art：physiology of transcranial motor cortex stimulation. *Brain Stiml* **1**：345-362, 2008
6) Rossini PM, et al：Non-invasive electrical and magnetic stimulation of the brain, spinal cord and roots：basic principles and procedures for routine clinical application. Report of an IFCN committee. *Electroenceph Clin Neurophysiol* **91**：79-92, 1994
7) Ugawa Y, et al：Magnitec stimulation of the corticospinal pathway at foramen magnum levels in humans. *Ann Neurol* **36**：618-624, 1994
8) Inghilleri M, et al：Silent period evoked by transcranial stimulation of the human cortex and cervicomedullary junction. *J Physiol* **466**：521-534, 1993
9) Kujirai T, et al：Corticocortical inhibition in the motor cortex. *J Physiol* **471**：501-519, 1993
10) Reis J, Swayne OB, Vandermeeren Y, et al：Contribution of transcranial magnetic stimulation to the understanding of cortical mechanisms involved in motor control. *J Physiol* **586**：325-351, 2008
11) Koch G, Schneider S, Baumer T, et al：Altered dorsal premotor-motor interhemispheric pathway activity in focal arm dystonia. *Mov Disord* **23**：660-668, 2008
12) Ugawa Y, Terao Y, Hanajima R, et al：Magnetic stimulation over the cerebellum in patients with ataxia. *Electroenceph clin Neurophysiol* **104**：453-458, 1997
13) Pascual-Leone A, et al：Akinesia in Parkinson's disease. Ⅱ. Shortening of choice reaction time and movement time with subthreshold repetitive transcranial motor cortex stimulation. *Neurology* **44**：892-898, 1994
14) Paulus W, Classen J, Cohen LG, et al：State of the art：pharmacologic effects on cortical excitability measures tested by transcranial magnetic stimulation. *Brain Stim* **1**：151-163, 2008
15) Daskalaskis ZJ, et al：Reduced cerebellar inhibition in schizoherenia：a preliminary study. *Am J Psychiatry* **152**：1203-1205, 2005
16) Hufnagel A, et al：Activation of the epileptic focus by

transcranial magnetic stimulation of the human brain. *Ann Neurol* **27**：49-60, 1990
17) Rossi S, Hallett M, Rossini PM, et al：The Safety of TMS Consensus Group：safety, ethical consideration, and application guidelines for use of transcranial magnetic stimulation in clinical practice and research. *Clin Neurophysiol* **120**：2008-2039, 2009
18) 磁気刺激法に関する委員会：磁気刺激法に関する委員会報告 No. 10. 臨神生 **34**：71-72, 2006

理学療法ジャーナル
1部定価 1,785円(本体1,700円+税5%)
年間購読 好評受付中！(学割有)
電子版もお選びいただけます
▶2011年9月号 [Vol.45 No.9]
特集 足部・足関節の機能と理学療法
特集記事
足／足関節のなりたち—バイオメカニカルな観点から／内山英一
下腿・足関節・足部の運動連鎖と病態運動学／園部俊晴
足部・足関節の機能障害とリハビリテーション／塚原秀明
足部・足関節の機能と転倒—つまずきやすさを表す足部クリアランスの観点から／小林吉之
足部・足関節の義肢装具による機能支援／阿部 薫
主要目次
入門講座 理学療法と「てこ」・1
「てこ」の原理／田中千歳
講座 理学療法スタンダード・1
脳卒中早期(急性期)の理学療法スタンダード／鵜飼正二、他
1ページ講座
理学療法関連用語：「除細動器」／櫻田弘治
義肢装具：「プラスチックKAFO」／日野 工
臨床実習サブノート スーパーバイザーの視点・論点—患者さんに触れるまで・6
ACL損傷または半月板損傷／舌間秀雄
最近の特集テーマ(2011年)
8月号 糖尿病の理学療法
7月号 神経生理学的アプローチの転換
6月号 小児理学療法の新たなる展開
5月号 がん患者のリハビリテーションと理学療法
4月号 ロコモティブシンドローム
医学書院
〒113-8719 東京都文京区本郷1-28-23
[販売部]TEL：03-3817-5657 FAX：03-3815-7804
E-mail：sd@igaku-shoin.co.jp http://www.igaku-shoin.co.jp 振替：00170-9-96693
携帯サイトはこちら

MRI-Based Correction for Partial-Volume Effect Improves Detectability of Intractable Epileptogenic Foci on ^{123}I-Iomazenil Brain SPECT Images

Hiroki Kato[1], Eku Shimosegawa[1], Naohiko Oku[2], Kazuo Kitagawa[3], Haruhiko Kishima[4], Youichi Saitoh[4], Amami Kato[5], Toshiki Yoshimine[4], and Jun Hatazawa[1]

[1]Department of Nuclear Medicine and Tracer Kinetics, Osaka University Graduate School of Medicine, Suita, Japan; [2]Department of Nuclear Medicine, Hyogo College of Medicine, Nishinomiya, Japan; [3]Department of Neurology, Osaka University Graduate School of Medicine, Suita, Japan; [4]Department of Neurosurgery, Osaka University Graduate School of Medicine, Suita, Japan; and [5]Department of Neurosurgery, Kinki University School of Medicine, Osaka-Sayama, Japan

^{123}I-Iomazenil brain SPECT has been used for the detection of epileptogenic foci, especially when surgical intervention is considered. Although epileptogenic foci exhibit a decrease in ^{123}I-iomazenil accumulation, normal cerebral cortices often exhibit similar findings because of thin cortical ribbons, gray matter atrophy, or pathologic brain structures. In the present study, we created ^{123}I-iomazenil SPECT images corrected for gray matter volume using MRI and tested whether the detectability of the epileptogenic foci improved. **Methods:** Seven patients (1 male patient and 6 female patients; mean age ± SD, 34 ± 17 y) with intractable epilepsy were surgically treated by resecting the cerebral cortex after surface electroencephalography. Histopathologic examination of the resected specimens and a good outcome after surgery indicated that the resected lesions were epileptogenic foci. These patients underwent ^{123}I-iomazenil SPECT and 3-dimensional T1-weighted MRI examinations before their operations. Each SPECT image was coregistered to the corresponding MR image, and its partial-volume effect (PVE) was corrected on a voxel-by-voxel basis with a smoothed gray matter distribution image. Four nuclear medicine physicians visually evaluated the ^{123}I-iomazenil SPECT images with and without the PVE correction. The SPECT count ratio of the suspected focus to the contralateral cerebral cortex was evaluated as an asymmetry index (%) based on the volume of interest. **Results:** The sensitivity, specificity, and accuracy of focus detection by visual assessment were higher after PVE correction (88%, 99%, and 98%, respectively) than before correction (50%, 92%, and 87%, respectively). The mean asymmetry index for the surgically resected lesions was significantly higher on the PVE-corrected SPECT images (22%) than on the PVE-uncorrected ones (16%) (P = 0.006). **Conclusion:** MRI-based PVE correction for ^{123}I-iomazenil brain SPECT improves the sensitivity and specificity of the detection of cortical epileptogenic foci in patients with intractable epilepsy.

Key Words: epilepsy; ^{123}I-iomazenil; SPECT; MRI; partial-volume effect

J Nucl Med 2008; 49:383–389
DOI: 10.2967/jnumed.107.046136

Iomazenil labeled with ^{123}I is a tracer that is specifically bound to central benzodiazepine receptors (*1*). Because epileptogenic foci exhibit a reduction in central benzodiazepine receptors (*2,3*), ^{123}I-iomazenil brain SPECT has been used to detect epileptic foci, especially when surgical intervention is considered (*3*). However, normal cerebral cortices often exhibit similar findings on ^{123}I-iomazenil SPECT because of thin cortical ribbons, gray matter atrophy, or pathologic brain structures. This limitation is caused by the partial-volume effect (PVE), which arises from the limited spatial resolution of the scanner. In small structures, the observed radioactivity concentration differs from the true concentration because of blurring of the counts out of the structure ("spill-out") and blurring of the counts into the structure from the surrounding radioactivity ("spill-in") (*4*).

In a previous study (*5*) examining patients with intractable mesial temporal lobe epilepsy arising from hippocampal sclerosis, the sensitivity of detecting pathologic hippocampi using ^{11}C-flumazenil PET was improved by PVE correction using MRI-based measurements of hippocampal volume. In the present study, we created ^{123}I-iomazenil SPECT images corrected for the whole-brain gray matter volume based on MRI measurements in patients with intractable partial epilepsy and tested whether the detectability of cortical epileptogenic foci improved.

MATERIALS AND METHODS

Patients

Seven patients with intractable epilepsy (1 male patient and 6 female patients; mean age ± SD, 34 ± 17 y) who met the following criteria were studied: no morphologic brain lesions other than small

Received Aug. 7, 2007; revision accepted Nov. 20, 2007.
For correspondence or reprints contact: Jun Hatazawa, MD, PhD, Osaka University Graduate School of Medicine, 2-2 Yamadaoka, Suita, 565-0871, Japan.
E-mail: hatazawa@tracer.med.osaka-u.ac.jp
COPYRIGHT © 2008 by the Society of Nuclear Medicine, Inc.

cystic lesions or suspected unilateral hippocampal atrophy (hippocampal sclerosis) visible on routine conventional MR images, surgical removal and histopathologic examination of suspected epileptogenic foci, improvement of patients' symptoms after surgery, and performance of ^{123}I-iomazenil brain SPECT and 3-dimensional (3D) T1-weighted MRI studies before operation.

The patients' clinical information is summarized in Table 1. All patients had complex partial seizures with or without generalization and were being treated with anticonvulsants. The Wada test, verbal magnetoencephalogram, or Edinburgh test was performed to determine the lateralization of verbal function or memory. All patients underwent surface electroencephalography or magnetoencephalography to identify the location and extent of the epileptogenic foci. All specimens resected during the operations were histopathologically investigated (Table 2). The histologic findings in 5 of 7 patients were nonspecific gliosis or neurodegeneration, and 1 patient (patient 3) was suspected of having astrocytoma. The outcome after surgery was evaluated on the basis of Engel's classification. The average follow-up period after surgery was 14 mo (range, 9–18 mo). Five patients were classified as Engel's classification I, and the remaining patients as Engel's classification III.

SPECT

In each subject, 167 MBq of ^{123}I-iomazenil were intravenously administered. Three hours after the injection, SPECT images were acquired while the subject rested supine on the scanning bed with eyes closed in a quiet room. SPECT was performed using a 4-head γ-camera (*6*) (Gamma View SPECT 2000H; Hitachi Medical Corp.) with a low-energy middle-resolution thin-section parallel-hole collimator. After the patient's head had been fixed on the headrest, the orbitomeatal line was detected using a laser-assisted device equipped with the γ-camera. The acquisition protocol was 20 s per step, with 64 collections over 360°, and the data were recorded in a 64 × 64 matrix. The raw SPECT data were transferred to a nuclear medicine computer (HARP 3; Hitachi Medical Corp.). The projection data were prefiltered using a Butterworth filter (cutoff frequency, 0.20 cycles per pixel; order, 10) and reconstructed into transaxial sections of 4.0-mm thickness in planes parallel to the orbitomeatal line. Attenuation correction was performed using Chang's method (*7*) with an optimized effective attenuation coefficient of 0.08 cm^{-1}.

PVE Correction

PVE was corrected using 3D T1-weighted MRI and a personal computer (Dell Dimension 8300; Dell Inc.) running Windows XP (Microsoft Corp.), as described in Figure 1. Thin-slice sagittal 3D T1-weighted MR images were produced using 3 types of MRI scanners: a Signa Excite 3.0 T, a Signa Excite HD 1.5 T (GE Yokogawa Medical Systems Ltd.), and a Magnetom Vision Plus 1.5 T (Siemens AG). In each case, a spoiled gradient echo sequence was used (echo time/repetition time: 1.928/8.632 ms, 1.820/8.552 ms, and 4.700/9.000 ms for the respective scanners; flip angle: 18, 18, and 12, respectively; acquisition matrix: all 256 × 256; slice thickness: all 1.4 mm). The acquired sagittal images were reformatted to axial images with a thickness of 1.4 mm.

The T1-weighted MR images were first segmented into gray matter, white matter, cerebrospinal fluid, or other compartments (skull and extracranial structures) using SPM5 (Wellcome Department of Imaging Neuroscience). This procedure yielded a Bayesian probability map for each tissue class based on a priori MRI information with an inhomogeneity correction for the magnetic field (*8*). Voxels were assigned into 3 tissue classes (gray matter, white matter, and cerebrospinal fluid) according to the maximum probability encountered for each voxel across the 3 datasets. These 3 tissue classes were subsequently put into binary form (given a value of 0 for absence of tissue or 1 for presence of tissue) (*9*).

The point-spreading function of the reconstructed SPECT images acquired with the low-energy middle-resolution thin-section parallel-hole collimator was assessed using a ^{123}I 1-mm-diameter line source in air, according to a previously described methodology (*6*). The binary maps for the gray matter were convoluted with a 3D gaussian function with a full width at half maximum of 12 × 12 × 12 mm, which was assumed to be the same as the point-spreading function of the reconstructed SPECT image, as described in previous studies (*10,11*). The resulting image was subsequently referred to as the smoothed gray matter map.

The ^{123}I-iomazenil SPECT images were coregistered to the smoothed gray matter maps using FMRIB's Linear Image Registration Tool (FLIRT) (*12*). In this procedure, the ^{123}I-iomazenil SPECT images were simultaneously reformatted to a matrix of the same size (256 × 256 × 256) as the referenced smoothed gray matter maps.

A binary volume image was created from the smoothed gray matter map as a mask image for the gray matter. The threshold for determining

TABLE 1
Characteristics of Subjects

Patient no.	Age (y)	Sex	Onset (y)	Duration (y)	Seizures/mo	Interval* (d)	Diagnosis	Anticonvulsants	MRI	Language dominancy
1	24	F	14	10	120	4	LTLE	CBZ, CLB	NP	L (Wada test)
2	65	F	43	22	30	2	MTLE	PHT	NP	Bilateral (Wada test)
3	44	F	40	4	30	2	LTLE	None	Small cyst in R ATL	Bilateral (Wada test)
4	14	F	3	11	5	10	MTLE	VPA, CBZ, PHT	NP	L (MEG study)
5	30	F	8	22	10	7	MTLE	CBZ, CLB, CZP	R HS	L (Wada test)
6	28	F	19	9	5	3	MTLE	VPA	L HS	L (Edinburgh test)
7	31	M	9	22	8	2	LTLE	CBZ, CLB, CZP	NP	R (Wada test)

*Between last seizure and SPECT study.

LTLE = lateral temporal lobe epilepsy; CBZ = carbamazepine; CLB = clobazam; NP = not performed; MTLE = mesial temporal lobe epilepsy; PHT = phenytoin; ATL = anterior temporal lobe; VPA = sodium valproate; MEG = magnetoencephalogram; CZP = clonazepam; HS = hippocampal sclerosis.

TABLE 2
Operations and Prognosis

Patient no.	Resected lesions	Histology	Prognosis*	Follow-up (mo)
1	L superior temporal gyrus, middle temporal gyrus (corticectomy/multiple subpial transection)	Gliosis	IIc	18
2	L hippocampus (multiple subpial transection), L superior temporal gyrus (corticectomy)	Gliosis	Ib	17
3	R anterior temporal lobe (tailored lobectomy), R hippocampus (hippocampectomy)	Astrocytoma	Ia–Ib	16
4	R hippocampus (hippocampectomy), temporal lobe (tailored corticectomy)	Gliosis, degeneration	Id	14
5	R hippocampus (hippocampectomy), anterior temporal lobe (tailored lobectomy), superior temporal gyrus (corticectomy)	Satellitosis	Ia	14
6	L hippocampus (hippocampectomy), amygdaloid (amygdaloidectomy)	Neurodegeneration	Ia	9
7	L posterior central gyrus, angular gyrus (selective corticectomy/multiple subpial transection)	Unknown	IIIa	9

*Engel's classification. Class I: free of disabling seizures (completely seizure-free since surgery [Ia], nondisabling simple partial seizures [Ib], some disabling seizures but free of disabling seizures for at least 2 y ["running down"] [Ic], generalized convulsion with antiepileptic drug withdrawal only [Id]). Class II: rare disabling seizures (rare disabling seizures since surgery [<3/y] [IIa], more than rare disabling seizures initially but only rare seizures for at least 2 y [IIb], nocturnal seizures only [IIc]). Class III: worthwhile improvement (significant reduction in seizure frequency [>75% reduction] [IIIa], prolonged seizure-free intervals amounting to greater than half the follow-up period of at least 2 y [IIIb]). Class IV: no worthwhile improvement (insignificant reduction, no change, or increase in seizure frequency).

the boundary of the binary volume image was set at 35% (an empirically determined value) of the maximum, which was the same as the threshold value used in a previous study (*10*). This mask image for the gray matter was then applied to the coregistered ^{123}I-iomazenil SPECT image. The masked ^{123}I-iomazenil SPECT image was then divided using the smoothed gray matter map on a pixel-by-pixel basis (Fig. 1).

Visual Assessment

Four experienced nuclear medicine physicians visually assessed the coronal images. The physicians were unaware of the patients' clinical information to avoid biases caused by differences in the amount of information available for each of the patients. The physicians visually evaluated the coronal ^{123}I-iomazenil SPECT images with and without PVE correction, presented in a random order, and noted the areas of epileptogenic foci, where the tracer uptake was reduced when compared with the corresponding contralateral regions. Decisions on the foci were made by joint agreement during a conference of the 4 physicians.

Patients without epileptogenic foci were excluded from the present study. Therefore, the sensitivity and specificity of focus

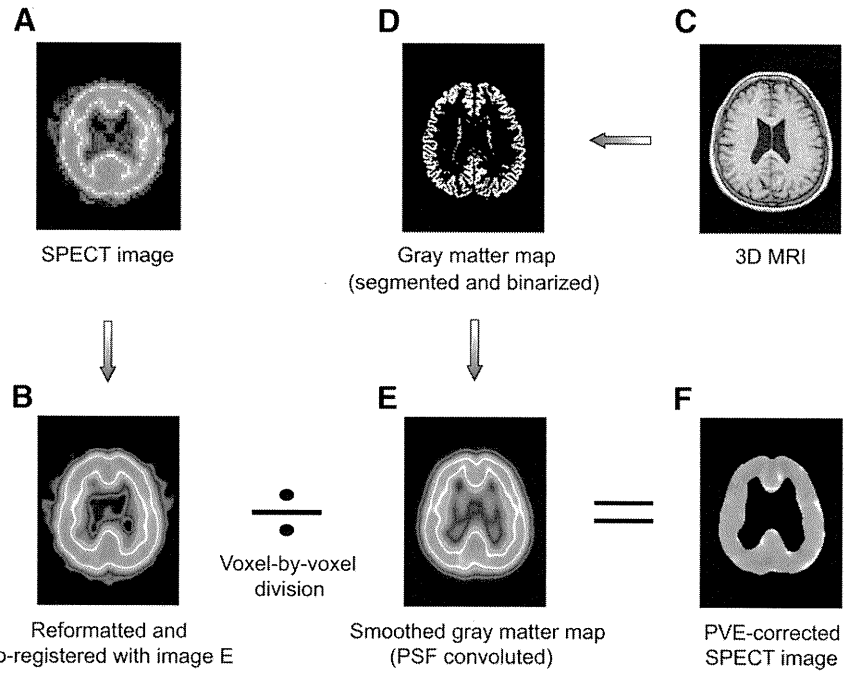

FIGURE 1. (A) ^{123}I-Iomazenil SPECT image. (B) Automatic coregistration of ^{123}I-iomazenil SPECT image with MR image via smoothed gray matter maps. Maps were simultaneously reformatted to matrix that was same size as referenced smoothed gray matter map. (C) 3D MR image obtained before operation. (D) MR image segmented into Bayesian probability map showing 3 tissue classes. Gray matter probability map was subsequently put into binary form (0 for absence of tissue, 1 for presence of tissue). (E) Binary map for gray matter convoluted with point-spreading function (PSF), which was assumed to be same as point-spreading function of SPECT scanner. (F) Smoothed gray matter map masked with threshold set to 35% of maximum voxel value. Coregistered ^{123}I-iomazenil SPECT image was divided using masked smoothed gray matter map on voxel-by-voxel basis.

detection were determined on a region-by-region basis. We divided the whole cerebrum into 18 bilateral blocks, as shown in Figure 2. We then assigned a binary value of positive or negative to each block, based on the visual assessment (i.e., positive for a focus, negative for no focus). We assumed that the resected lesions corresponded to the true epileptogenic foci and that unresected regions corresponded to the intact brain, because follow-up of surgical outcomes of the patients was good. Then, a true-positive result was defined as a positive result of visual assessment in a resected brain region, a true-negative result was defined as a negative result of visual assessment in an unresected brain region, a false-positive result was defined as a positive result of visual assessment in an unresected brain region, and a false-negative result was defined as a negative result of visual assessment in a resected brain region. The sensitivity, specificity, and accuracy of uncorrected or PVE-corrected SPECT images were calculated as follows:

$$\text{sensitivity} = \text{number of true-positive blocks/number of resected blocks},$$

$$\text{specificity} = \text{number of true-negative blocks/number of unresected blocks},$$

$$\text{accuracy} = (\text{number of true-positive blocks} + \text{number of true-negative blocks})/\text{number of total blocks}.$$

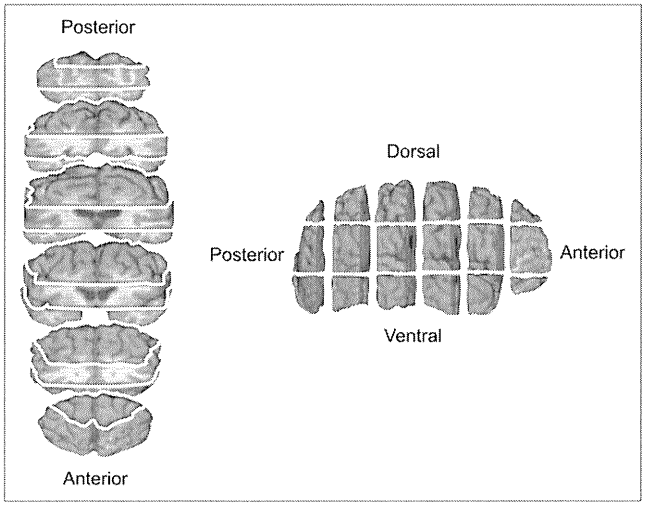

FIGURE 2. Whole cerebrum was divided into 18 bilateral blocks. A binary value of positive or negative was assigned to each block on the basis of visual assessment (i.e., positive for focus, negative for no focus). In this study, we assumed that resected lesions corresponded to true epileptogenic foci and unresected regions corresponded to intact brain because of good follow-up outcomes of patients after operations. Then, result of evaluation of each block was defined as follows. true-positive: positive result of visual assessment in resected brain region; true-negative: negative result of visual assessment in unresected brain region; false-positive: positive result of visual assessment in unresected brain region; false-negative: negative result of visual assessment in resected brain region.

Quantitative Assessment

First, the volume of interest (VOI) was established so as to include each resected lesion in reference to an MR image obtained after the operation (Fig. 3). If the VOI included a medial temporal lesion, it was divided into a medial temporal and a lateral part. Second, another VOI was made so as to contain each visually detected false-positive area on the uncorrected or PVE-corrected SPECT images that were coregistered with the MR images. For each of these VOIs, the corresponding contralateral VOI was also made in reference to the SPECT and MR images. The VOI counts of the uncorrected or the PVE-corrected SPECT images coregistered with the MR images were measured to evaluate quantitatively the sensitivity or specificity of the images of the epileptogenic foci. The asymmetry index (AI) for the ^{123}I-iomazenil SPECT count of the ipsilateral VOI A, C_A, and that of the contralateral VOI B, C_B, was calculated as follows:

$$\text{AI} = |C_A - C_B| \times 200/(C_A + C_B). \qquad \text{Eq. 1}$$

RESULTS

The sensitivity, specificity, and accuracy of focus detection by visual assessment were higher after PVE correction (88%, 99%, and 98%, respectively) than before correction (50%, 92%, and 87%, respectively). The AI values for the resected lesions are summarized in Table 3. The mean AI was significantly higher on the PVE-corrected SPECT images than on the uncorrected ones for the whole resected lesions (22%, 16%, $P = 0.006$), lateral parts of the resected lesions (20%, 12%, $P = 0.006$), and medial temporal parts of the resected lesions (25%, 20%, $P = 0.029$). In patients 2 and 7, true foci were not detected on the uncorrected SPECT images. In Table 4, the location, visual assessment, and AI for the false-positive regions are listed. The mean AI for the false-positive regions was significantly larger on the uncorrected images (12%) than on the PVE-corrected ones (4.8%) ($P < 0.001$).

The uncorrected and PVE-corrected SPECT images of typical patients are shown in Figure 4. A lateralized decrease in the counts was found on the PVE-corrected images in the areas corresponding to the resected lesions, although no laterality was seen on the uncorrected images (Fig. 4A). Conversely, a lateralized decrease in the counts was seen in the intact areas on the uncorrected images, whereas no laterality was found on the PVE-corrected images (Fig. 4B).

DISCUSSION

In the present study, we introduced a method for performing MRI-based PVE corrections on ^{123}I-iomazenil SPECT images. This method improved the accuracy with which epileptogenic foci can be detected in the cerebral cortices.

Inhibitory neural transmission is thought to be disturbed at epileptic foci (*13*). This hypothesis is supported by in vivo flumazenil PET (*14,15*) and iomazenil SPECT (*2,3*) studies. Previous studies have indicated a disproportion between the gray matter volume and the benzodiazepine receptor density in some epileptogenic foci (*3,16,17*). In patients with hippocampal sclerosis, changes in benzodiazepine receptor

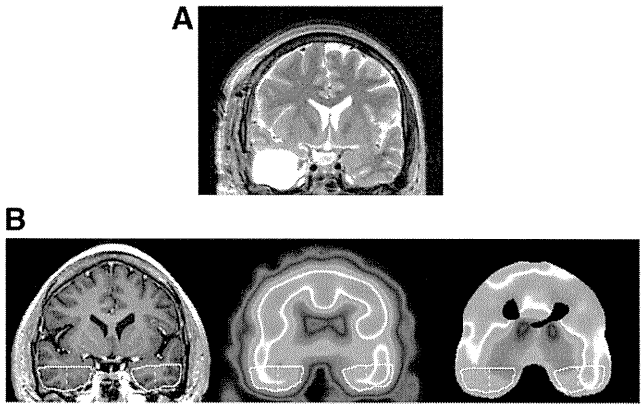

FIGURE 3. (A) MR image obtained after operation. (B) VOIs for resected brain lesions were established on 3D MR image (left) so as to include each resected lesion in reference to MR image obtained after operation. Corresponding contralateral VOIs were also established on same MR image. If VOI included medial temporal area, it was divided into lateral temporal part and medial temporal part (dashed line). Each VOI was applied to uncorrected (middle) and PVE-corrected (right) SPECT images coregistered to 3D MR image.

binding were detected in the hippocampus and the extrahippocampal neocortices, which appeared normal on MRI (*18*). Thus, identifying the location of epileptogenic foci and evaluating the extent of the area to be resected may be impossible using MRI alone. In the present study, a considerable number of true-positive lesions in the cerebral cortices appeared normal during the MRI study.

The nonspecific binding of iomazenil has been shown to account for a small proportion of all bound molecules (1%–3%) (*19*). According to an ex vivo study of nonhuman primates, iomazenil showed a predominantly high accumulation in the gray matter, with ratios of greater than 30:1 for gray matter to white matter (*20*). Thus, the distribution of iomazenil accumulation in the cerebrum is markedly influenced by the local volume of gray matter when a SPECT scanner with a limited spatial resolution is used. Nonpathologic laterality or an asymmetric distribution of gray matter volume on a certain slice may increase the risk of a false-positive result in side-by-side comparisons of iomazenil images.

The accurate determination of actual radiotracer concentrations in human gray matter in vivo is possible using MRI-based PVE corrections (*21,22*). In ethylcysteinate dimer SPECT, PVE correction made the regional cerebral blood flow distribution more homogeneous throughout the brain, with less intersubject variation than in the original distribution. Using this method for brain perfusion SPECT determines regional cerebral blood flow more accurately, even in healthy volunteers (*10*). As for ^{15}O-H_2O PET, PVE correction made it possible to estimate the regional cerebral blood flow accurately despite cortical atrophy both in Alzheimer's disease (*23*) and in normal aging (*24*). In ^{18}F-FCWAY (^{18}F-*trans*-4-fluoro-*N*-2-[4-(2-methoxyphenyl)piperazin-1-yl]ethyl-*N*-(2-pyridyl)cyclohexanecarboxamide) PET for the detection of foci in TLE patients, MRI-based PVE correction effectively eliminated artifacts related to PVE that were influenced by the local geometry of the gray matter and was useful for the extraction of pathologic serotonin 1A binding reduction (*25*).

The MRI-based PVE correction method used in the present study is similar to that used in previous studies (*5,10,23,26*). In this study, PVE was corrected for gray matter and other components (2-compartment method), although the PVE correction was performed for gray matter, white matter, and other brain structures (3-compartment method) in most of the previous studies. According to a previous validation study (*21*), the 2-compartment method is less sensitive to errors resulting from resolution mismatch between MRI and SPECT, misregistration, and missegmentation. Meanwhile, the 3-compartment method is capable of greater accuracy for absolute quantitative measures. The accumulation of ^{123}I-iomazenil in white matter is known to be markedly small; consequently, the spill-in of counts from the surrounding white matter to the gray matter voxels is negligible. For this application, the 2-compartment method is more suitable because the decrease in accuracy is small and the tolerance to errors in image processing is greater with the 2-compartment method than with the 3-compartment one.

TABLE 3
AI for VOI Counts in Resected Lesions

Patient no.	Resected lesions	Total resected lesions (AI [%])		Lateral part of lesions (AI [%])		Medial temporal part of lesions (AI [%])	
		Uncorrected	PVE-corrected	Uncorrected	PVE-corrected	Uncorrected	PVE-corrected
1	STG, MTG	2.2	10.8	2.2	10.8	—	—
2	ATL, MTL	7.4	13.6	5.6	13.0	−0.2	10.8
3	ATL, MTL	21.7	34.4	21.3	34.2	9.6	15.3
4	ITG, MTL	29.5	38.7	24.7	34.5	39.4	46.4
5	ATL, MTL	12.2	14.6	10.0	13.2	21.1	22.5
6	MTL	27.8	30.6	—	—	27.8	30.6
7	IPL	9.1	11.6	9.1	11.6	—	—

STG = superior temporal gyrus; MTG = middle temporal gyrus; ATL = anterior temporal lobe; MTL = mesial temporal lobe; ITG = inferior temporal gyrus; IPL = inferior parietal lobule.

TABLE 4
AI for VOI in False-Positive Areas

Patient no.	Location	Uncorrected		PVE-corrected	
		Visual assessment	AI (%)	Visual assessment	AI (%)
1	ATL	Positive	15.0	Positive	13.1
2	MTL-WM*	Positive	10.7	Negative	2.1
	SPL	Positive	10.3	Negative	4.1
3	OG	Positive	11.1	Negative	7.2
	IPL	Positive	14.6	Negative	1.4
	SPL	Positive	10.1	Negative	4.6
5	PHG	Positive	12.0	Negative	1.2
6	ATL	Positive	13.6	Negative	7.3
7	SPL	Positive	11.6	Negative	2.1
	MTL	Positive	11.9	Negative	4.7

*Contralateral to true focus.

ATL = anterior temporal lobe; MTL-WM = mesial temporal lobe white matter; SPL = superior parietal lobule; OG = orbital gyri; IPL = inferior parietal lobule; PHG = parahippocampal gyrus; MTL = mesial temporal lobe.

In this study, an increase in the AI of the resected lesions was shown after PVE correction in both the lateral part and medial temporal part of the resected lesions. This finding implies an increase in the volume of the gray matter or decrease in the volume of the adjacent white matter in the lesion areas, compared with that in the corresponding contralateral normal areas. In the previous study (*27*), an increase in the regional gray matter concentration in malformations of cortical development in patients with focal cortical dysplasia was detected by voxel-based morphometry. In addition, the local increase of the gray matter volume has been reported to coincide with that of the white matter volume, as detected by voxel-based morphometry, around pathologic sclerotic medial temporal lesions in cases of temporal lobe epilepsy (*28*). This phenomenon may, however, be controversial, and further detailed investigation is needed of the changes in the AI in pathologic medial temporal lesions associated with PVE correction.

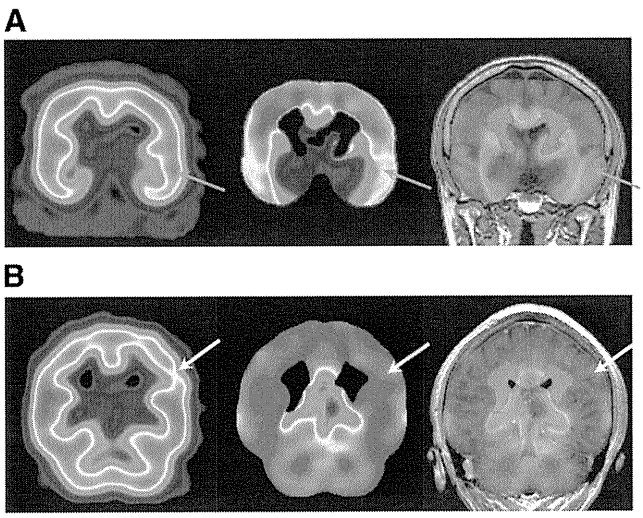

FIGURE 4. Typical SPECT images of 2 patients are shown. In each case, uncorrected SPECT image is on left, PVE-corrected SPECT image in middle, and PVE-corrected SPECT image coregistered to MR image on right. (A) Although no laterality could be found on uncorrected images, localized decrease in count on PVE-corrected images is distinct in areas corresponding to resected lesions. (B) No laterality was found on PVE-corrected images; unilateral decreased count, however, was found in intact areas on uncorrected images. Arrows indicate the true focus (red) or the false-positive region (yellow).

The present study had some limitations. First, the number of patients was too small to ensure statistical reliability. Second, some of the patients were taking anticonvulsants (e.g., clobazam) at the time of their ^{123}I-iomazenil SPECT examination, even though such drugs may influence iomazenil binding to a certain extent. Previous reports, however, have suggested that the extent of this influence is small (*3,29*). Thus, as far as intrasubject comparisons using the AI are concerned, the influence of anticonvulsants was thought to be negligible. Additionally, the temporary withdrawal of anticonvulsants solely for the purpose of SPECT can be harmful or impractical. From this viewpoint, our findings suggest that PVE corrections for ^{123}I-iomazenil SPECT remain effective even when the patient is taking anticonvulsants. Third, the brain structure images were obtained using 3 different types of MRI scanners. However, this protocol was not problematic in the present study because interscanner comparisons were not included in the analysis. Fourth, white matter activity was masked and eliminated during the process of PVE correction, although some cases of refractory focal epilepsy with heterotopia caused by neuronal migration disturbances have been reported to show a high flumazenil uptake in periventricular white matter (*30*). Because the evaluation of abnormal ^{123}I-iomazenil activity in white matter is quite difficult because of the higher activity spill-out from the adjacent gray matter, further study to solve this problem is needed. Fifth, the resolution of the present scanner was around 11 mm, although the current state-of-the-art SPECT scanner has a resolution of around 4–5 mm at full width at half maximum. We consider that the PVE correction in these scanners is effective to detect small cortical foci of epilepsy. Finally, we assumed that the unresected brain tissues were normal. Because this assumption cannot be proved, the accuracy of the true-negative and false-positive categorizations is limited.

CONCLUSION

PVE correction for ^{123}I-iomazenil brain SPECT images using the MRI-based gray matter volume improved the sensitivity and specificity at which cortical epileptogenic foci could be detected in patients with intractable epilepsy.

ACKNOWLEDGMENTS

We thank the staffs of the Department of Pathology, Osaka University Graduate School of Medicine, for their help with the histology; Dr. Yasuyuki Kimura, Dr. Katsufumi Kajimoto,

and Dr. Makiko Tanaka for their contribution to the SPECT data acquisition; and Yukio Nakamura and the staff of the Department of Nuclear Medicine and the cyclotron staff of Osaka University Hospital for their technical support in performing this study. This study was supported in part by a grant for molecular imaging project from the Japan Science Technology Agency.

REFERENCES

1. Beer HF, Blauenstein PA, Hasler PH, et al. In vitro and in vivo evaluation of iodine-123-Ro 16-0154: a new imaging agent for SPECT investigations of benzodiazepine receptors. *J Nucl Med.* 1990;31:1007–1014.
2. Morimoto K, Watanabe T, Ninomiya T, et al. Quantitative evaluation of central-type benzodiazepine receptors with [^{125}I]iomazenil in experimental epileptogenesis: II. The rat cortical dysplasia model. *Epilepsy Res.* 2004;61: 113–118.
3. Sata Y, Matsuda K, Mihara T, Aihara M, Yagi K, Yonekura Y. Quantitative analysis of benzodiazepine receptor in temporal lobe epilepsy: [^{125}I]iomazenil autoradiographic study of surgically resected specimens. *Epilepsia.* 2002;43: 1039–1048.
4. Hoffman EJ, Huang SC, Phelps ME. Quantitation in positron emission computed tomography: 1. Effect of object size. *J Comput Assist Tomogr.* 1979;3: 299–308.
5. Koepp MJ, Richardson MP, Labbe C, et al. ^{11}C-Flumazenil PET, volumetric MRI, and quantitative pathology in mesial temporal lobe epilepsy. *Neurology.* 1997;49:764–773.
6. Kimura K, Hashikawa K, Etani H, et al. A new apparatus for brain imaging: four-head rotating gamma camera single-photon emission computed tomograph. *J Nucl Med.* 1990;31:603–609.
7. Chang LT. A method for attenuation correction in radionuclide computed tomography. *IEEE Trans Nucl Sci.* 1978;25:638–643.
8. Ashburner J, Friston KJ. Voxel-based morphometry: the methods. *Neuroimage.* 2000;11:805–821.
9. Bencherif B, Stumpf MJ, Links JM, Frost JJ. Application of MRI-based partial-volume correction to the analysis of PET images of mu-opioid receptors using statistical parametric mapping. *J Nucl Med.* 2004;45:402–408.
10. Matsuda H, Ohnishi T, Asada T, et al. Correction for partial-volume effects on brain perfusion SPECT in healthy men. *J Nucl Med.* 2003;44:1243–1252.
11. Ibanez V, Pietrini P, Alexander GE, et al. Regional glucose metabolic abnormalities are not the result of atrophy in Alzheimer's disease. *Neurology.* 1998;50: 1585–1593.
12. Jenkinson M, Smith S. A global optimisation method for robust affine registration of brain images. *Med Image Anal.* 2001;5:143–156.
13. Savic I, Persson A, Roland P, Pauli S, Sedvall G, Widen L. In-vivo demonstration of reduced benzodiazepine receptor binding in human epileptic foci. *Lancet.* 1988;2:863–866.
14. Arnold S, Berthele A, Drzezga A, et al. Reduction of benzodiazepine receptor binding is related to the seizure onset zone in extratemporal focal cortical dysplasia. *Epilepsia.* 2000;41:818–824.
15. Juhasz C, Chugani DC, Muzik O, et al. Relationship of flumazenil and glucose PET abnormalities to neocortical epilepsy surgery outcome. *Neurology.* 2001;56:1650–1658.
16. Lamusuo S, Pitkanen A, Jutila L, et al. [^{11}C]Flumazenil binding in the medial temporal lobe in patients with temporal lobe epilepsy: correlation with hippocampal MR volumetry, T2 relaxometry, and neuropathology. *Neurology.* 2000; 54:2252–2260.
17. Hammers A, Koepp MJ, Richardson MP, et al. Central benzodiazepine receptors in malformations of cortical development: a quantitative study. *Brain.* 2001;124: 1555–1565.
18. Hammers A, Koepp MJ, Labbe C, et al. Neocortical abnormalities of [^{11}C]-flumazenil PET in mesial temporal lobe epilepsy. *Neurology.* 2001;56:897–906.
19. Videbaek C, Friberg L, Holm S, et al. Benzodiazepine receptor equilibrium constants for flumazenil and midazolam determined in humans with the single photon emission computer tomography tracer [^{123}I]iomazenil. *Eur J Pharmacol.* 1993;249:43–51.
20. Sybirska E, al-Tikriti M, Zoghbi SS, Baldwin RM, Johnson EW, Innis RB. SPECT imaging of the benzodiazepine receptor: autoradiographic comparison of receptor density and radioligand distribution. *Synapse.* 1992;12:119–128.
21. Meltzer CC, Kinahan PE, Greer PJ, et al. Comparative evaluation of MR-based partial-volume correction schemes for PET. *J Nucl Med.* 1999;40:2053–2065.
22. Muller-Gartner HW, Links JM, Prince JL, et al. Measurement of radiotracer concentration in brain gray matter using positron emission tomography: MRI-based correction for partial volume effects. *J Cereb Blood Flow Metab.* 1992;12: 571–583.
23. Meltzer CC, Leal JP, Mayberg HS, Wagner HN Jr, Frost JJ. Correction of PET data for partial volume effects in human cerebral cortex by MR imaging. *J Comput Assist Tomogr.* 1990;14:561–570.
24. Meltzer CC, Cantwell MN, Greer PJ, et al. Does cerebral blood flow decline in healthy aging? A PET study with partial-volume correction. *J Nucl Med.* 2000; 41:1842–1848.
25. Giovacchini G, Toczek MT, Bonwetsch R, et al. 5-HT 1A receptors are reduced in temporal lobe epilepsy after partial-volume correction. *J Nucl Med.* 2005;46: 1128–1135.
26. Koepp MJ, Woermann FG. Imaging structure and function in refractory focal epilepsy. *Lancet Neurol.* 2005;4:42–53.
27. Bonilha L, Montenegro MA, Rorden C, et al. Voxel-based morphometry reveals excess gray matter concentration in patients with focal cortical dysplasia. *Epilepsia.* 2006;47:908–915.
28. Bernasconi N, Duchesne S, Janke A, Lerch J, Collins DL, Bernasconi A. Whole-brain voxel-based statistical analysis of gray matter and white matter in temporal lobe epilepsy. *Neuroimage.* 2004;23:717–723.
29. Duncan S, Gillen GJ, Brodie MJ. Lack of effect of concomitant clobazam on interictal ^{123}I-iomazenil SPECT. *Epilepsy Res.* 1993;15:61–66.
30. Hammers A, Koepp MJ, Richardson MP, Hurlemann R, Brooks DJ, Duncan JS. Grey and white matter flumazenil binding in neocortical epilepsy with normal MRI: a PET study of 44 patients. *Brain.* 2003;126:1300–1318.